ICAS 2021 SHANGHAI
32nd Congress of the International Council of the Aeronautical Sciences
September 6-10, 2021 Pudong Shangri-La, Shanghai, China

DESIGN OF UAV NAVIGATION ALGORITHM IN SINGLE SATELLITE ENVIRONMENT BASED ON HIGH PRECISION TIMING

Ketao Li[1], Hangshuai Ma[1], Dan Wang[1]

1 China National Aeronautical Radio Electronics Research Institute

Abstract

Global Navigation Satellite System (GNSS) is playing an important role for the unmanned aerial vehicle (UAV), and the theoretical research, technical framework and application of GNSS-based navigation have been well developed. However, there is also a serious problem is that GNSS can not work when the UAV encircled in a round of special environment (e.g. indoor physical environment, urban street canyon and poor weather conditions) because of the challenge of GNSS signal unavailability. In order to compensate for this issue, a new efficient navigation algorithm based on the chip scale atomic clock (CSAC) is mentioned in this paper.

Keywords: Chip scale atomic clock; Single satellite environment; Tightly coupled integrated navigation; Rejected satellite navigation

1. Introduction

Global navigation satellite system (GNSS) based on radio signals is widely used for vehicles, robots and pedestrians, also for the unmanned aerial vehicle (UAV). With the help of GNSS, UAV can locate its position (e.g. roadway, woods and buildings) in physical environment conveniently. However, in some cases, the signals of satellite are easily disturbed by occlusion and interference, so there are less than four satellites even only one which is used for navigation, which is called navigation interruption by (Groves, P.D. 2013). The so called navigation interruption makes it difficult to provide continuous position information to high-speed moving UAV.

An integrated navigation system combining GNSS and inertial navigation systems (INS) is an effective way to overcome the problem, the integration system can offer high precision, small volume, good reliability, low dynamic stress sensitivity, and no error accumulation. At present there are three types of integration navigation systems, including loosely coupled, tightly coupled, and ultra-tightly coupled configurations. In loosely coupled system, the GNSS measured velocity and position are used to integrate with the velocity and position of INS. It is the simplest integration mode, however, the method requires at least four satellites. For tightly coupled system, the raw pseudo-range and pseudo-range rate measurements of GNSS are directly used in the data fusion algorithm to estimate and correct the INS bias, therefore, the system is able to achieve a higher accuracy even the number of available satellites is insufficient for single point positioning. For the ultra-tightly coupled system, INS is the auxiliary system to aid the GNSS in the tracking domain, while the theory of ultra-tightly coupled system remains unclear and has not been applied. So in this paper, the research is based on the tightly coupled INS/GNSS integrated navigation system.

In addition, a new generation of Atomic clocks, are now commercially available. Their power consumption, price and size have been reduced considerably in the last years. This tendency is driving GNSS providers to incorporate one of these clocks into their high-end products in order to improve the performance of their navigation solution and provide the most-precise frequency reference for humans. GNSS receivers normally include a Temperature Compensated Cristal Oscillator (TCXO) clock, and this unit exhibits a noisy short-term stability and a poor long-term stability. To overcome the long-term instability, TCXO clocks are time disciplined with the satellites' atomic clocks. The CSAC can solve the problem of short-term stability, but they are also affected by a long-term instability. A combination of CSAC short-term stability and the GNSS disciplined long-term stability will result in better navigation performance under the numerous conditions which was documented in (Bruggemann et al. 2006). USA National Institute of Standard and Technology fabricated the CSAC in 2002 . And the CSAC technology was developed by the Defense Advanced Research Projects Agency (DARPA). The size, weight, power, and cost of CSAC are obviously better than those of classical Atomic Clocks. (Preston 2015) described a CSACs typical accuracy is 10-10 per second at start up, improving to 10-12 per second after several seconds of GNSS disciplining .

Commercialization of CSAC extends the applications of atomic clocks. For positioning and navigation applications, CSAC can improve positioning accuracy. It also can be regarded as a satellite for GNSS. (Van Graas 1992), (Kline 1997), and (Bednarz 2004) found that classical rubidium clocks have the ability to improve positioning accuracy of GNSS. Recently, (David Calero 2015), and (T. Krawinkel 2015) presented that benefits of CSAC in GNSS applications. (Ma 2015) and (Ma 2016) proposed that deeply coupled CSAC and GNSS can improve positioning, navigation, and timing (PNT) robustness and explored the coupled integration of CSAC, MIMU, and GNSS for PNT performance .

Researching the measurement of solving the problem mentioned in the first paragraph based on the integration of CSAC, MIMU, and GNSS has become a hotspot in the field of navigation. Thus, this study contributes to a new integration navigation system based on CSAC to provide continuous and high-accuracy position information to moving carriers in some emergency conditions that UAV can only receive signals from one or two satellites.

2. Theory Basis

2.1 Clock Error Modelling

Generally speaking, a clock is an oscillator which can generate a sinusoidal signal with a given nominal frequency coupled with a frequency counter. The deviation of the real from the nominal frequency is composed of frequency offset, drift, and random frequency fluctuations. The difference between the clock's time and nominal time t, which is called the clock error δt, can be approximated by (1):

$$\delta t = m_0 + m_1\left(t - t_0\right) + m_2\left(t - t_0\right)^2 + x\left(t, t_0\right) \tag{1}$$

Where m_0 is systematic time offset, m_1 is the frequency offset, m_2 is the frequency drift, $t - t_0$ represents clock coasting time, and $x\left(t, t_0\right)$ is the random noise. Thus, a quadratic polynomial can be used to describe the main (deterministic) part of a clock model.

(T. Krawinkel 2015) computed two different solutions in order to establish appropriate models for GNSS data analysis and apply the knowledge gained about the devices' frequency stabilities: (i) modeling the process noise in an EKF, (ii) applying a clock polynomial in a sequential least-squares adjustment (SLSA). A description of the EKF algorithm can be found in (T. Krawinkel 2014). The SLSA is basically pretty similar to the Kalman filter. The main difference the estimation results are only based on GNSS observations. Therefore, the clock error of receiver at epoch k is defined as the following equation, we follow (2):

$$\delta t_k = \sum_{i=0}^{n} m_i \Delta t^i \tag{2}$$

Where m_i refers to the unknown coefficients for time offset $\left(i = 0\right)$, frequency offset $\left(i = 1\right)$, and frequency drift $\left(i = 2\right)$, respectively, and Δt^i reflects the length of the clock modeling interval.

Normally, a linear polynomial is enough to be used to account for time and frequency offset. While for some clocks an additional quadratic term can be more reasonable.

2.2 Architecture of Coupled Integration

To carry out this study, a CSAC SA.45S from Microsemi, a STIM300 MIMU, a GNSS receiver OEM-638 from Novatel, a navigation processor, a portable power, and several interfaces are used. The outside view of these elements are shown in Figure 1, The physical structure of the integration navigation system consisted of all of these elements is shown in Figure 2.

Figure 3 describe a more specific architecture of coupled integration, which includes four blocks: GNSS, INS, timing, and precise time-aiding navigation filter. The timing block provides clock signals for others blocks. The GNSS block (receive signal from only one satellite), in turn, determines the start time of CSAC. One pulse per second (1 PPS) signal enters the timing block, and so called "clock coasting" in CSAC restrains clock error accumulation and reduces the noise of 1 PPS signal by using a feedback loop which contains a digital phase detector, regulator, CSAC, and frequency division. In the precise time-aiding navigation filter block, pseudo range, pseudo range rate, INS output, and precise time are the input data. Integration state and observation models are constructed based on precise time, and the Kalman filter is used to integrate navigation information. Finally, the error parameters are corrected and the calibrated data is transmitted back to sensors. The PNT information is provided as the integration of navigation system's output.

Figure 1 – The outside view of CSAC、MIMU and GNSS receiver.

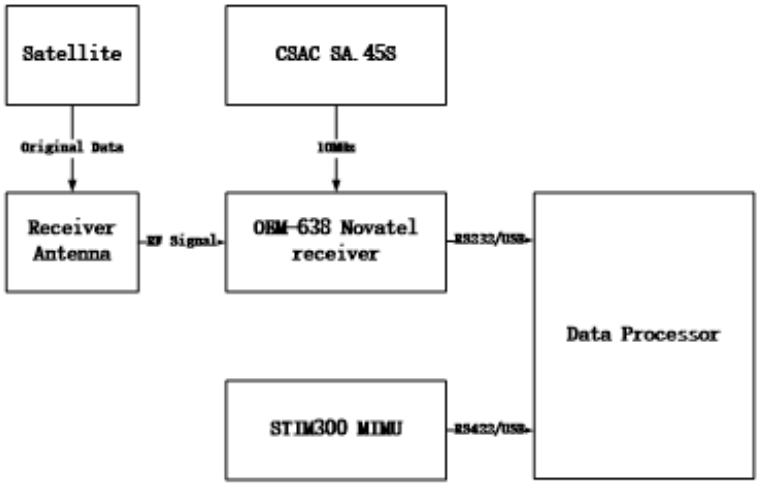

Figure 2 – The physical structure of the coupled integration.

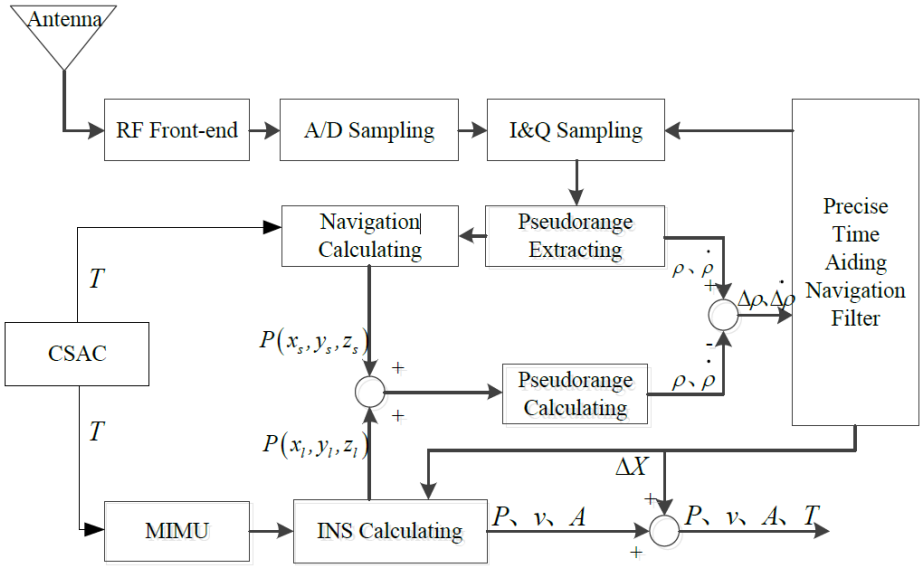

Figure 3 – Architecture of chip scale atomic clock (CSAC), MEMS inertial measurement unit (MIMU), and global navigation satellite system (GNSS) coupled integration.

3. Mathematical Model of Navigation Filter

The precise time-aiding coupled navigation filter is based on the Kalman filter. Specifically, the integration state model is constructed by inertial sensors (gyroscope and accelerometer), the integration observation model is constructed by GNSS information, and all above work with precise time aiding.

3.1 Integration State Model

The state vector $\mathbf{X}$ can be defined as (3):

$$\boldsymbol{X}=\begin{bmatrix}\boldsymbol{\phi} & \boldsymbol{\delta R} & \boldsymbol{\delta V} & \boldsymbol{\varepsilon} & \nabla & \boldsymbol{\delta K}_g & \boldsymbol{\delta K}_a\end{bmatrix}^T \tag{3}$$

Where $\boldsymbol{\phi}=\begin{bmatrix}\phi_E & \phi_N & \phi_U\end{bmatrix}$ is the error of pitch, roll, and yaw angles; $\boldsymbol{\delta R}=\begin{bmatrix}\delta\lambda & \delta L & \delta h\end{bmatrix}$ is the error of latitude, longitude, and altitude of MIMU; $\delta\boldsymbol{V}=\begin{bmatrix}\delta v_E & \delta v_N & \delta v_U\end{bmatrix}$ is the error of east, north, and up velocity; $\boldsymbol{\varepsilon}=\begin{bmatrix}\varepsilon_x & \varepsilon_y & \varepsilon_z\end{bmatrix}$ is the three-axis gyroscope bias; $\nabla=\begin{bmatrix}\nabla_x & \nabla_y & \nabla_z\end{bmatrix}$ is the three-axis accelerometer bias; $\delta\boldsymbol{K}_g=\begin{bmatrix}\delta k_{gx} & \delta k_{gy} & \delta k_{gz}\end{bmatrix}$ is the scale factor error of the gyroscopes; and $\delta\boldsymbol{K}_a=\begin{bmatrix}\delta k_{ax} & \delta k_{ay} & \delta k_{az}\end{bmatrix}$ is the scale factor of the accelerometers. Compare with the state model of traditional tightly coupled integrated navigation system, clock bias and drift are not treated as state variables in this model because of the precise time aiding.

Therefore, the state equation is obtained:

$$\dot{\boldsymbol{X}}=\boldsymbol{F}\cdot\boldsymbol{X}+\boldsymbol{W} \tag{4}$$

Where $\boldsymbol{F}$ is the state matrix, and $\boldsymbol{W}$ is the state noise.

3.2 Integration Observation Model

Range Measurement Error

Suppose that the real position of the carrier is $\boldsymbol{R}_0=\begin{bmatrix}x_0 & y_0 & z_0\end{bmatrix}^T$, the position of the carrier calculated by the MIMU is $\boldsymbol{R}_{MIMU}=\begin{bmatrix}x_{MIMU} & y_{MIMU} & z_{MIMU}\end{bmatrix}^T$, the number of satellites which can be received by the receiver is $N=1,2,...n$ and the position of the nth satellite is $\boldsymbol{R}_{(n)}=\begin{bmatrix}x_{(n)} & y_{(n)} & z_{(n)}\end{bmatrix}^T$.

So the pseudo-range between the carrier calculated by the MIMU and the satellite can be written as:

$$\rho_{MIMU}^{(n)}=\left|\boldsymbol{R}_{(n)}-\boldsymbol{R}_{MIMU}\right|=\sqrt{\left(x_{(n)}-x_{MIMU}\right)^2+\left(y_{(n)}-y_{MIMU}\right)^2+\left(z_{(n)}-z_{MIMU}\right)^2} \tag{5}$$

Meanwhile, the real range between the real position of the carrier and the satellite is:

$$r_0^{(n)}=\left|\boldsymbol{R}_{(n)}-\boldsymbol{R}_0\right|=\sqrt{\left(x_{(n)}-x_0\right)^2+\left(y_{(n)}-y_0\right)^2+\left(z_{(n)}-z_0\right)^2} \tag{6}$$

Taylor expansion of equation (7) is obtained as follow by neglecting higher order terms:

$$\rho_{MIMU}^{(n)}=r_0^{(n)}+\frac{x_{(n)}-x_0}{r_0^{(n)}}\delta x+\frac{y_{(n)}-y_0}{r_0^{(n)}}\delta y+\frac{z_{(n)}-z_0}{r_0^{(n)}}\delta z \tag{7}$$

The pseudo-range between the carrier and satellite provided by the GNSS receiver with the precise time aiding is:

$$\rho_{GNSS}^{(n)}=r_0^{(n)}+\varepsilon_{\delta t_u}+\varepsilon_c^{(n)} \tag{8}$$

Where $\varepsilon_c^{(n)}$ is the error of position, which include the satellite clock offset, ephemeris errors, ionosphere delay, troposphere delay, and multipath error except the receiver clock noise. $\varepsilon_{\delta t_u}$ is the error of position caused by the receiver clock noise.

Thus, the range measurement error is:

$$\begin{aligned}\delta\rho^{(n)} &= \rho_{GNSS}^{(n)} - \rho_{MIMU}^{(n)} \\ &= -\left(\frac{x_{(n)}-x_0}{r_0^{(n)}}\delta x + \frac{y_{(n)}-y_0}{r_0^{(n)}}\delta y + \frac{z_{(n)}-z_0}{r_0^{(n)}}\delta z\right) + \varepsilon_c^{(n)} + \varepsilon_{\delta tu} \\ &= -\begin{bmatrix}\frac{x_{(n)}-x_0}{r_0^{(n)}} & \frac{y_{(n)}-y_0}{r_0^{(n)}} & \frac{z_{(n)}-z_0}{r_0^{(n)}}\end{bmatrix}\begin{bmatrix}\delta x\\ \delta y\\ \delta z\end{bmatrix} + \varepsilon_c^{(n)} + \varepsilon_{\delta tu}\end{aligned} \tag{9}$$

Where

$$\begin{bmatrix}\delta x\\ \delta y\\ \delta z\end{bmatrix} = \boldsymbol{C}_g^e\begin{bmatrix}R\cos L\delta\lambda\\ R\delta L\\ \delta h\end{bmatrix} = \left(\boldsymbol{C}_e^g\right)^{-1}\begin{bmatrix}R\cos L & 0 & 0\\ 0 & R & 0\\ 0 & 0 & 1\end{bmatrix}\begin{bmatrix}\delta\lambda\\ \delta L\\ \delta h\end{bmatrix} \tag{10}$$

When the visible satellites' number is N , The range measurement error can be indicated as:

$$\boldsymbol{\delta\rho} = \boldsymbol{M}\begin{bmatrix}\delta x\\ \delta y\\ \delta z\end{bmatrix} + \boldsymbol{\varepsilon_c} + \boldsymbol{\varepsilon_{\delta tu}} \tag{11}$$

Where

$$\boldsymbol{\delta\rho} = \begin{bmatrix}\delta\rho^{(1)}\\ \delta\rho^{(2)}\\ \vdots\\ \delta\rho^{(N)}\end{bmatrix},\quad \boldsymbol{M} = \begin{bmatrix}\frac{x_0-x_{(1)}}{r_0^{(1)}} & \frac{y_0-y_{(1)}}{r_0^{(1)}} & \frac{z_0-z_{(1)}}{r_0^{(1)}}\\ \frac{x_0-x_{(2)}}{r_0^{(2)}} & \frac{y_0-y_{(2)}}{r_0^{(2)}} & \frac{z_0-z_{(2)}}{r_0^{(2)}}\\ \vdots & \vdots & \vdots\\ \frac{x_0-x_{(N)}}{r_0^{(N)}} & \frac{y_0-y_{(N)}}{r_0^{(N)}} & \frac{z_0-z_{(N)}}{r_0^{(N)}}\end{bmatrix},\quad \boldsymbol{\varepsilon_c}+\boldsymbol{\varepsilon_{\delta tu}} = \begin{bmatrix}\varepsilon_c^{(1)}+\varepsilon_{\delta tu}\\ \varepsilon_c^{(2)}+\varepsilon_{\delta tu}\\ \vdots\\ \varepsilon_c^{(N)}+\varepsilon_{\delta tu}\end{bmatrix} \tag{12}$$

Range Rate Measurement Error

The derivative of formula (6) and (7) with time can be written as:

$$\dot r_0^{(n)} = \frac{\left(x_{(n)}-x_0\right)\left(\dot x_{(n)}-\dot x_0\right)+\left(y_{(n)}-y_0\right)\left(\dot y_{(n)}-\dot y_0\right)+\left(z_{(n)}-z_0\right)\left(\dot z_{(n)}-\dot z_0\right)}{r_0^{(n)}} \tag{13}$$

$$\begin{aligned}\dot\rho_{MIMU}^{(n)} &= \dot r_0^{(n)} + \left(\frac{\dot x_{(n)}-\dot x_0}{r_0^{(n)}} - \frac{\left(x_{(n)}-x_0\right)\dot r_0^{(n)}}{\left(r_0^{(n)}\right)^2}\right)\delta x + \left(\frac{\dot y_{(n)}-\dot y_0}{r_0^{(n)}} - \frac{\left(y_{(n)}-y_0\right)\dot r_0^{(n)}}{\left(r_0^{(n)}\right)^2}\right)\delta y \\ &+ \left(\frac{\dot z_{(n)}-\dot z_0}{r_0^{(n)}} - \frac{\left(z_{(n)}-z_0\right)\dot r_0^{(n)}}{\left(r_0^{(n)}\right)^2}\right)\delta z + \frac{x_{(n)}-x_0}{r_0^{(n)}}\delta\dot x + \frac{y_{(n)}-y_0}{r_0^{(n)}}\delta\dot y + \frac{z_{(n)}-z_0}{r_0^{(n)}}\delta\dot z\end{aligned} \tag{14}$$

Where, $\delta\dot x = \dot x_{MIMU} - \dot x_0$, $\delta\dot y = \dot y_{MIMU} - \dot y_0$, $\delta\dot z = \dot z_{MIMU} - \dot z_0$ are the vector's velocity error.

The derivative of range between carrier and the satellite from GNSS receiver with time is:

$$\dot\rho_{GNSS}^{(n)} = \dot r_0^{(n)} + \xi^{(n)} \tag{15}$$

$$\xi^{(n)} = \xi_{sat-orbit}^{(n)} + \xi_{sat-clock}^{(n)} + \xi_{sat-speed}^{(n)} + \xi_{t+i}^{(n)} + \xi_{rec-clock}^{(n)} + \xi_{rec-pos}^{(n)} + \xi_{rec-dop}^{(n)} \tag{16}$$

Where $\xi_{sat-orbit}^{(n)}$, $\xi_{sat-clock}^{(n)}$, $\xi_{sat-speed}^{(n)}$, $\xi_{t+i}^{(n)}$, $\xi_{rec-clock}^{(n)}$, $\xi_{rec-pos}^{(n)}$ and $\xi_{rec-dop}^{(n)}$ are the error of range rate caused by the satellite track error, satellite clock offset, satellite speed, ionosphere delay, troposphere delay, receiver clock offset, receiver position error and receiver doppler measurement error.

Thus, the derivative of the range measurement error can be written as:

$$\begin{aligned}\delta\dot{\rho}^{(n)} &= \dot{\rho}_{GNSS}^{(n)} - \dot{\rho}_{MIMU}^{(n)} = \xi^{(n)} \\ &-\left[\left(\frac{\dot{x}_{(n)}-\dot{x}_0}{r_0^{(n)}} - \frac{\left(x_{(n)}-x_0\right)\dot{r}_0^{(n)}}{\left(r_0^{(n)}\right)^2}\right)\delta x + \left(\frac{\dot{y}_{(n)}-\dot{y}_0}{r_0^{(n)}} - \frac{\left(y_{(n)}-y_0\right)\dot{r}_0^{(n)}}{\left(r_0^{(n)}\right)^2}\right)\delta y\right. \\ &\left.+\left(\frac{\dot{z}_{(n)}-\dot{z}_0}{r_0^{(n)}} - \frac{\left(z_{(n)}-z_0\right)\dot{r}_0^{(n)}}{\left(r_0^{(n)}\right)^2}\right)\delta z + \frac{x_{(n)}-x_0}{r_0^{(n)}}\delta\dot{x} + \frac{y_{(n)}-y_0}{r_0^{(n)}}\delta\dot{y} + \frac{z_{(n)}-z_0}{r_0^{(n)}}\delta\dot{z}\right]\end{aligned} \tag{17}$$

Normally, the correlation between the range rate error and the position error is extremely weak, so the equation (17) can be simplified as follow:

$$\delta\dot{\rho}^{(n)} = \xi^{(n)} - \left(\frac{x_{(n)}-x_0}{r_0^{(n)}}\delta\dot{x} + \frac{y_{(n)}-y_0}{r_0^{(n)}}\delta\dot{y} + \frac{z_{(n)}-z_0}{r_0^{(n)}}\delta\dot{z}\right) \tag{18}$$

When the visible satellites' number is N ,The range rate measurement error can be indicated as:

$$\boldsymbol{\delta\dot{\rho}} = \boldsymbol{M}\begin{bmatrix}\delta\dot{x}\\ \delta\dot{y}\\ \delta\dot{z}\end{bmatrix} + \boldsymbol{\xi} \tag{19}$$

Where

$$\boldsymbol{\delta\dot{\rho}} = \begin{bmatrix}\delta\dot{\rho}^{(1)}\\ \delta\dot{\rho}^{(2)}\\ \vdots\\ \delta\dot{\rho}^{(N)}\end{bmatrix}, \boldsymbol{\xi} = \begin{bmatrix}\xi^{(1)}\\ \xi^{(2)}\\ \vdots\\ \xi^{(N)}\end{bmatrix} \tag{20}$$

Observation Model

The observation equation is obtained:

$$\boldsymbol{Z} = \boldsymbol{C}\cdot\boldsymbol{X} + \boldsymbol{U} \tag{21}$$

Where the observation variable is:

$$\boldsymbol{Z} = \begin{bmatrix}\delta\boldsymbol{\rho}\\ \delta\boldsymbol{\dot{\rho}}\end{bmatrix}_{2N\times 1} \tag{22}$$

The observation matrix is:

$$\boldsymbol{C} = \begin{bmatrix} 0_{N\times 3} & \boldsymbol{M}\cdot\left(\boldsymbol{C}_e^g\right)^{-1}\begin{bmatrix}R\cos L & 0 & 0\\ 0 & R & 0\\ 0 & 0 & 1\end{bmatrix} & 0_{N\times 3} & 0_{N\times 3} & 0_{N\times 3} & 0_{N\times 3} & 0_{N\times 3} \\ 0_{N\times 3} & 0_{N\times 3} & \boldsymbol{M}\cdot\left(\boldsymbol{C}_e^g\right)^{-1} & 0_{N\times 3} & 0_{N\times 3} & 0_{N\times 3} & 0_{N\times 3}\end{bmatrix} \tag{23}$$

The observation noise is:

$$\boldsymbol{U} = \begin{bmatrix}\boldsymbol{\varepsilon}_{\delta_{tu}} + \boldsymbol{\varepsilon}_c\\ \boldsymbol{\xi}\end{bmatrix}_{2N\times 1} \tag{24}$$

4. Simulation and Verification

4.1 Flight Path Design

Figure 4 illustrates a simple flight path of a UAV which lasts for approximately 2150s, which conclude UAV's elementary motion such as stationary, speed up skating, climb, flat flight, turn, landing and slow down skating. The black, red and yellow ellipses mark three areas where the GNSS receiver can only obtain 1~3 satellites observation information. The UAV's attitude and speed in the whole flight phase are showed in the figure 5.

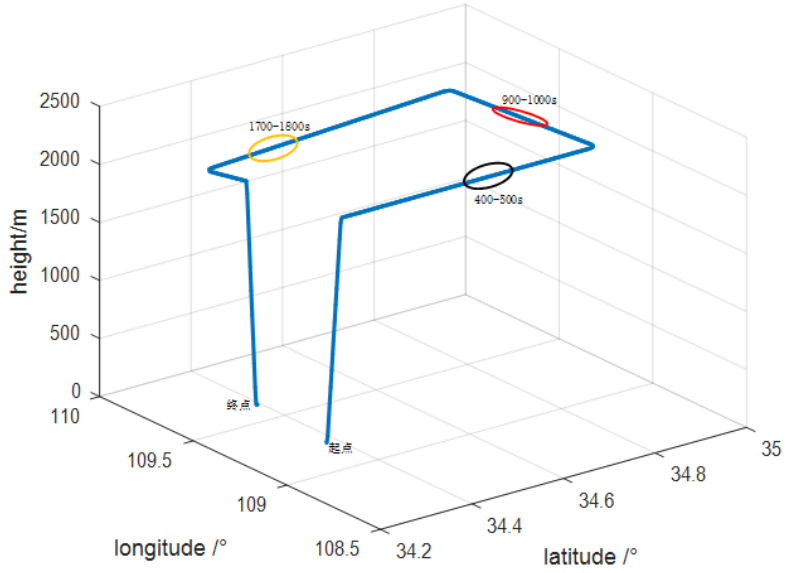

Figure 4 – The flight path of UAV.

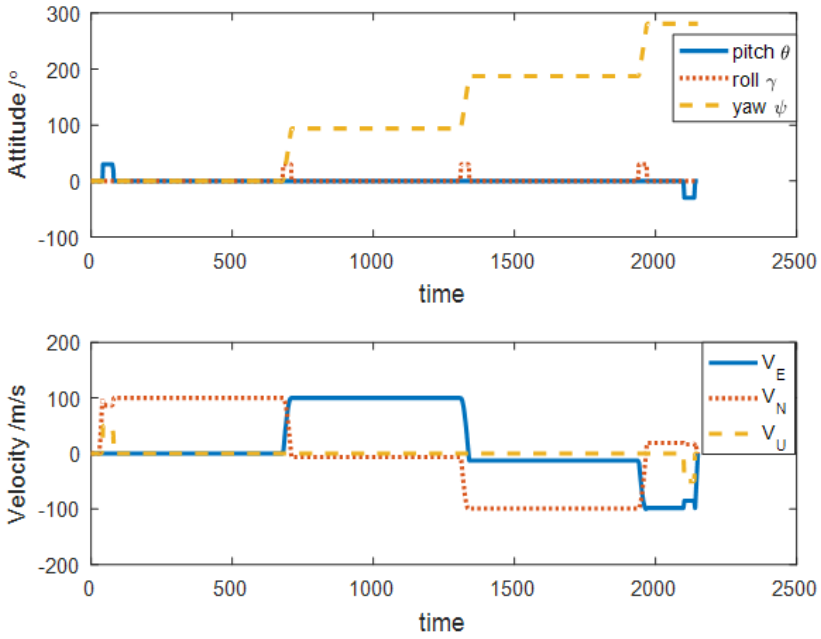

Figure 5 – The UAV's attitude and speed.

4.2 Simulation Condition and Parameter

Considering the UAV's background, we set the MIMU's device error in the table 1.

Sensor	Parameter	Value
Gyroscope	Constant Bias	$50^{\circ}/h$
	Random Walk Coefficient	$0.6^{\circ}/\sqrt{h}$
	Calibration Factor Error	1000PPM（1σ）
Accelerometer	Constant Bias	$1\times10^{-4}g$
	Random Walk Coefficient	$200\mu g/\sqrt{Hz}$
	Calibration Factor Error	1000PPM（1σ）

Table 1 – Main parameters of MIMU.

4.3 Open Environment

Suppose the UAV stay in the open environment during all the flight path. Figure 6 shows the tracked satellite number. The simulation navigation results are compared in Figure 7 and Table 2. The result of the coupled integration navigation of the demo setup “CSAC/MIMU/GNSS” was better than that obtained by another form. The horizontal positioning accuracy of “CSAC/MIMU/GNSS” (RMS) was 24.5% higher than that of “MIMU/GNSS” (RMS).

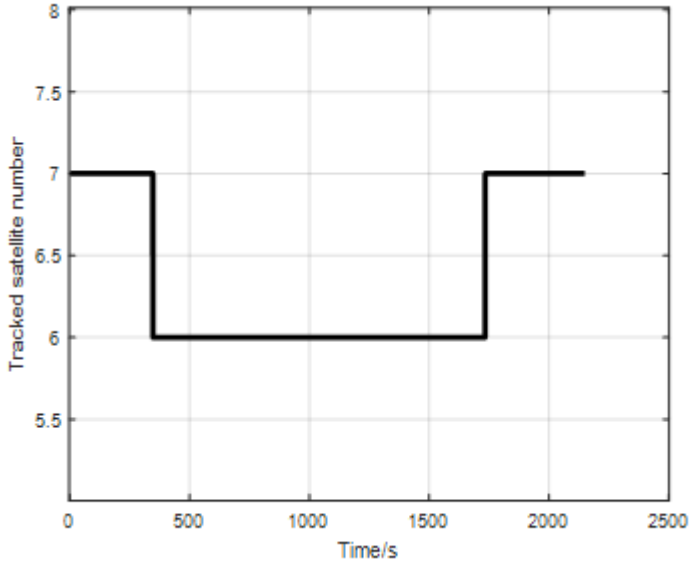

Figure 6 – Tracked satellite number.

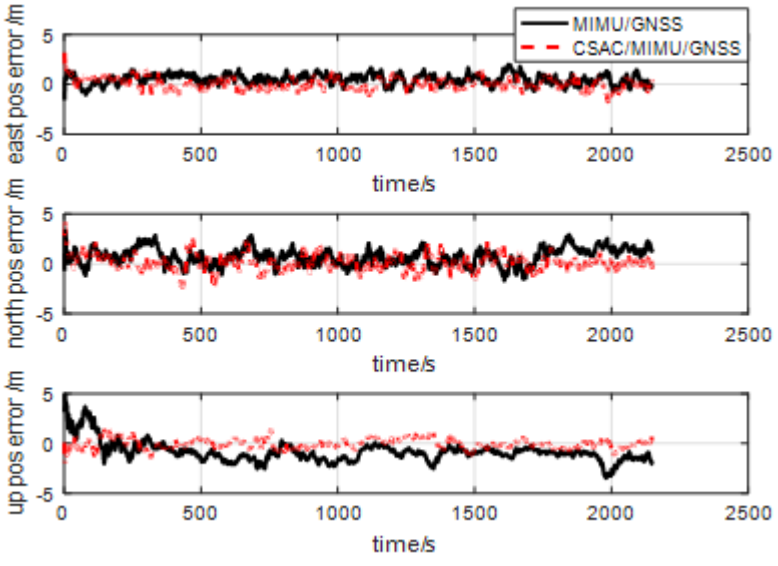

Figure 7 – Open environment comparison.

Mode	East/m	North/m	Horizontal/m
MIMU/GNSS	0.7149	1.1190	1.3279
CSAC/MIMU/GNSS	0.5733	0.8220	1.0022

Table 2 – Position error comparison in open environment (RMS).

4.4 Harsh Environment

Reduce the visible satellite number to only one when UAV fly in the black red and yellow areas. Figure 8 and table 3 illustrated the comparison of the navigation results. After application of the harsh environment, the positioning errors of “MIMU/GNSS” increased quickly with time, reaching >600 m at the end. The positioning errors of “CSAC/MIMU/GNSS” increased slowly and the horizontal error was 44.3942 m, which was more accurate than “MIMU/GNSS”. Figure 9 and table 4 showed that “CSAC/MIMU/GNSS” can still provide high accuracy positioning function when the visible satellite number is less than four. When the tracked satellite number is one, the horizontal positioning error of “CSAC/MIMU/GNSS” can be maintained about 100m in 100 seconds.

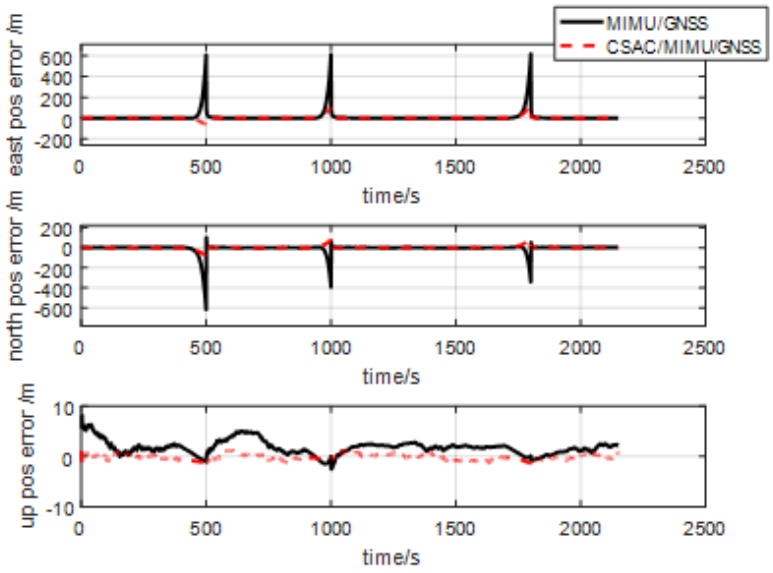

Figure 8 – Harsh environment comparison.

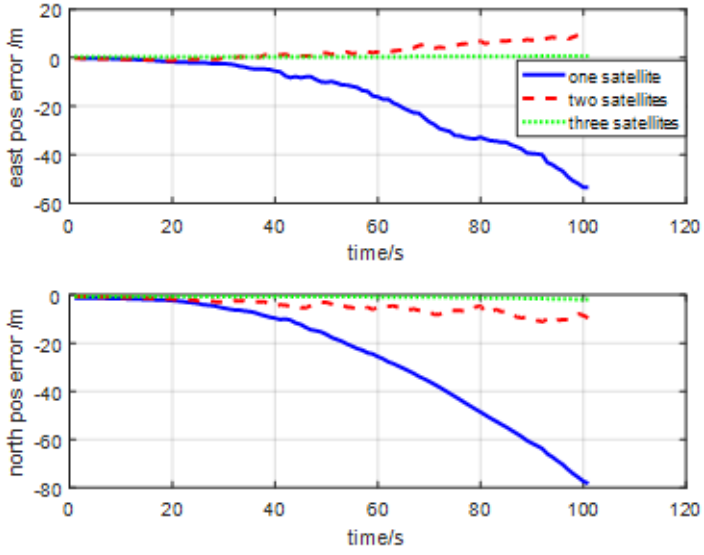

Figure 9 –Positioning error hold comparison.

Mode	East/m	North/m	Horizontal/m
MIMU/GNSS	161.7599	180.2606	242.1985
CSAC/MIMU/GNSS	26.4716	35.6384	44.3942

Table 3 – Position error comparison in harsh environment (RMS).

Tracked Satellite Number	Horizontal Positioning Error/m		
	100s	200s	300s
one	106.7155	1535.2	-
two	13.0385	34.1687	133.9819
three	2.0560	5.7158	25.0369

Table 4 –Horizontal position error comparison with different satellite number (MAX).

5. Conclusions

This paper discussed a new coupled integration of CSAC, MIMU, and GNSS applied in emergency conditions for the UAV based on single-satellite. The architecture of the integration was designed and the mathematical models of precise time aiding navigation filter were derived. A simulation was carried out to test and validate the system and the mathematical model of navigation filter. Results showed that the coupled integration was more accurate than the traditional techniques (the tightly coupled GNSS/MIMU) especially when the signals are disturbed. Therefore, the coupled integration of CSAC, MIMU, and GNSS can be used in some emergency conditions for the UAV and improve the PNT performance.

6. Contact Author Email Address

Ketao Li: weiwolkt@163.com

References

[1] Groves, P.D. The PNT Boom: Future Trends in Integrated Navigation. Inside GNSS, vol. 8, pp. 44-49, 2013.

[2] Microsemi GPS-2700 and GPS-2750 Datasheet (052112).

[3] Bruggemann, T. S., Greer, D. G and Walker, R. “Chip Scale Atomic Clocks: Benefits to Airborne GNSS Navigation Performance.”, International Global Navigation Satellite Systems Society IGNSS Symposium 2006.

[4] Lutwak, R. Chip-Scale Atomic Clock (Briefing Charts); Symmetricom-Technology Realization Center: Beverly, MA, USA, 2007.

[5] Preston, S., “GPS Multipath Detection and Mitigation Timing Bias Techniques”, Auburn University Thesis, pp. 21 & 49, 2015.

[6] Van Graas, F.; Braasch, M. GPS interferometric attitude and heading determination: Initial flight test results. Navigation, 38, 297–316,1992.

[7] Kline, P.A. Atomic Clock Augmentation for Receivers Using the Global Positioning System; Virginia Polytechnic Institute and State University: Blacksburg, VA, USA, 1997.

[8] Bednarz, S.G. Adaptive Modeling of GPS Receiver Clock for Integrity Monitoring during Precision Approaches; Massachusetts Institute of Technology: Cambridge, MA, USA, 2004.

[9] David, C, Enric F. Characterization of Chip-Scale Atomic Clock for GNSS navigation solutions, 2015 International Association of Institutes of Navigation World Congress Prague, Czech Republic, pp: 20–23, October 2015

[10]T. Krawinkel and S. Schön, "Application of Miniaturized Atomic Clocks in Kinematic GNSS Single Point Positioning," in Proceedings of the 28th European Frequency and Time Forum, Neuchatel, Switzerland,

2014.

[11]T. Krawinkel, S. Schön. Benefits of Chip Scale Atomic Clocks in GNSS Applications, In Proceedings of the 28th International Technical Meeting of the ION Satellite Division, Tampa, Florida, USA, 14-18; pp. 2867–2874, September 2015.

[12]Ma, L.; You, Z.; Li, B.; Zhou, B.; Han, R. Deep Coupled Integration of CSAC and GNSS for Robust PNT. Sensors, 15, 23050–23070, 2015.

[13]Ma, L.; You, Z.; Liu, T.Y.; Shi, S. Coupled Integration of CSAC, MIMU, and GNSS for Improved PNT Performance. Sensors, 16, 682, 2016.

Copyright Statement